POLITECNICO DI TORINO
Repository ISTITUZIONALE

Integrated Optimization of Layout and Inter-Array Cable Design for Floating Offshore Wind Farms

*Original*
Integrated Optimization of Layout and Inter-Array Cable Design for Floating Offshore Wind Farms / Dutto, L., Niosi, F., Carpinteri, M., Paduano, B., Garcia-Rosa, P.B., Imsland, L., Bracco, G.. - In: JOURNAL OF PHYSICS. CONFERENCE SERIES. - ISSN 1742-6588. - ELETTRONICO. - 3346:1(2026). [10.1088/1742-6596/3346/1/012030]

*Availability:*
This version is available at: 11583/3017524 since: 2026-11-04T15:57:01Z

*Publisher:*
IOP Publishing

*Published*
DOI:10.1088/1742-6596/3346/1/012030

*Terms of use:*

This article is made available under terms and conditions as specified in the corresponding bibliographic description in the repository

*Publisher copyright*

(Article begins on next page)

10 November 2026

Journal of Physics: Conference Series **3346** (2026) 012030 doi:10.1088/1742-6596/3346/1/012030

# Integrated Optimization of Layout and Inter-Array Cable Design for Floating Offshore Wind Farms

**Lorenzo Dutto[1], Francesco Niosi[1], Marco Carpinteri[1], Bruno Paduano[1], Paula B. Garcia-Rosa[2], Lars Imsland[3] and Giovanni Bracco[1]**

[1]MOREnergy Lab, Politecnico di Torino, Turin, Italy
[2]SINTEF Energy Research, Trondheim, Norway
[3]Department of Engineering Cybernetics, NTNU, Trondheim, Norway

E-mail: lorenzo.dutto@polito.it

**Abstract.** Floating offshore wind farms enable large-scale renewable energy generation in deep waters, where bottom-fixed solutions are not feasible. Their techno-economic performance depends on maximizing annual energy production while minimizing lifetime costs. In floating systems, turbine layout, inter-array cable routing, and depth-dependent mooring costs are strongly coupled. However, they are commonly optimized separately. This work presents a coupled layout–cable routing optimization framework based on a genetic algorithm. Cable routing is solved through a nested heuristic procedure, enabling explicit interaction between turbine placement, cable topology, and mooring costs. The genetic algorithm is benchmarked against a random search strategy to assess solution quality and computational cost. The framework is applied to a deep-water case study offshore Sicily (Italy), characterized by complex bathymetry. Results show that water depth variations and cable routing decisions significantly affect optimal layouts and cost distribution, highlighting the importance of integrated optimization for floating offshore wind farm design.

## 1 Introduction

Wind energy represents the largest share of variable renewable electricity worldwide [1]. Further expansion increasingly relies on offshore wind farms, which exploit stronger and more consistent wind resources. Floating offshore wind farms enable deployment in deep-water regions where bottom-fixed solutions are not feasible. However, their levelized cost of energy (LCOE) remains significantly higher than that of bottom-fixed offshore wind, requiring substantial cost reductions to achieve competitiveness.

Wind farm layout optimization (WFLO) plays a central role in improving techno-economic performance by maximizing annual energy production (AEP) or minimizing LCOE through optimal turbine placement under boundary, spacing, and wake constraints. While numerous studies incorporate aerodynamic, electrical, and economic aspects into WFLO, the influence of mooring system design has received comparatively limited attention.

In [2], turbine and mooring buffer zones are introduced to compare alternative mooring layouts under constant water depth. In [3], seabed variability is considered by adapting mooring line lengths and anchor positions for a six-turbine farm with simplified bathymetry. To date, [4] appears to be the only study integrating wake effects, mooring and anchor design, and cable routing within an LCOE minimization framework but considering only ten turbines and limited

Content from this work may be used under the terms of the Creative Commons Attribution 4.0 licence. Any further distribution of this work must maintain attribution to the author(s) and the title of the work, journal citation and DOI.
Published under licence by IOP Publishing Ltd

depth variations. Although these works highlight the importance of mooring design, the combined impact of turbine-specific, depth-dependent mooring optimization and inter-array cable routing optimization (IACRO) remains largely unexplored, particularly under the pronounced bathymetric gradients typical of deep-water Mediterranean sites.

This study proposes an integrated WFLO framework that simultaneously accounts for wake effects, turbine-specific mooring costs, and IACRO within a single LCOE objective function. Among the wide range of algorithms proposed in the literature [5, 6, 7], a genetic algorithm (GA) is adopted to optimize turbine positions. Optimal mooring configurations are precomputed and evaluated through a bottom-up cost model, while the cable routing is determined using the Esau–Williams heuristic within a nested optimization scheme.

The framework is applied to a case study offshore Sicily (Italy). First, a simplified gradient bathymetry is considered to isolate the interaction between mooring design and cable routing. Subsequently, the real bathymetry is used to assess the performance of the proposed framework under realistic conditions and to benchmark the GA against a random search (RS) approach.

The main contribution of this work is the integrated treatment of wake-driven productivity, depth-dependent mooring costs, and cable routing within a unified optimization framework. The case study quantifies their interplay and the resulting layout-driven cost reductions under realistic water-depth variability and farm scale.

The remainder of the paper is organized as follows. Section 2 presents the WFLO formulation and the GA and RS optimization frameworks together with the IACRO method, mooring model, and cost formulation. Section 3 describes the case study. Section 4 discusses the results for both bathymetry scenarios.

## 2 Methods

To capture the coupling between turbine layout, inter-array cable routing, and depth-dependent mooring costs, a nested optimization framework is adopted. Turbine positions are optimized in an outer loop, while cable routing and mooring costs are evaluated within each objective function call. Two search strategies are considered: a GA as the primary optimizer and an RS method as a benchmarking baseline.

The WFLO problem is formulated as a bounded continuous optimization problem. The design vector consists of the Cartesian coordinates of the $N$ turbines:

$$\mathbf{x} = (x_1, y_1, \ldots, x_N, y_N), \tag{1}$$

and the objective is to minimize the LCOE:

$$\min_{\mathbf{x}} \mathrm{LCOE}(\mathbf{x}). \tag{2}$$

The LCOE depends on the positioning of the turbines through three main contributions: AEP, accounting for wake interactions; depth-dependent mooring costs; and inter-array cable system costs obtained from a nested IACRO routine.

The wind farm domain is rectangular without exclusion zones (see Section 3). Feasible layouts satisfy box constraints,

$$x_{\min} \le x_i \le x_{\max}, \quad y_{\min} \le y_i \le y_{\max}, \quad i = 1, \ldots, N, \tag{3}$$

and a minimum inter-turbine spacing requirement. Layouts violating spacing constraints are penalized and excluded from detailed evaluation.

Figure 1 illustrates the GA framework emphasizing the objective evaluation loop. Prior to optimization, site conditions and turbine/substructure properties are defined. These inputs are

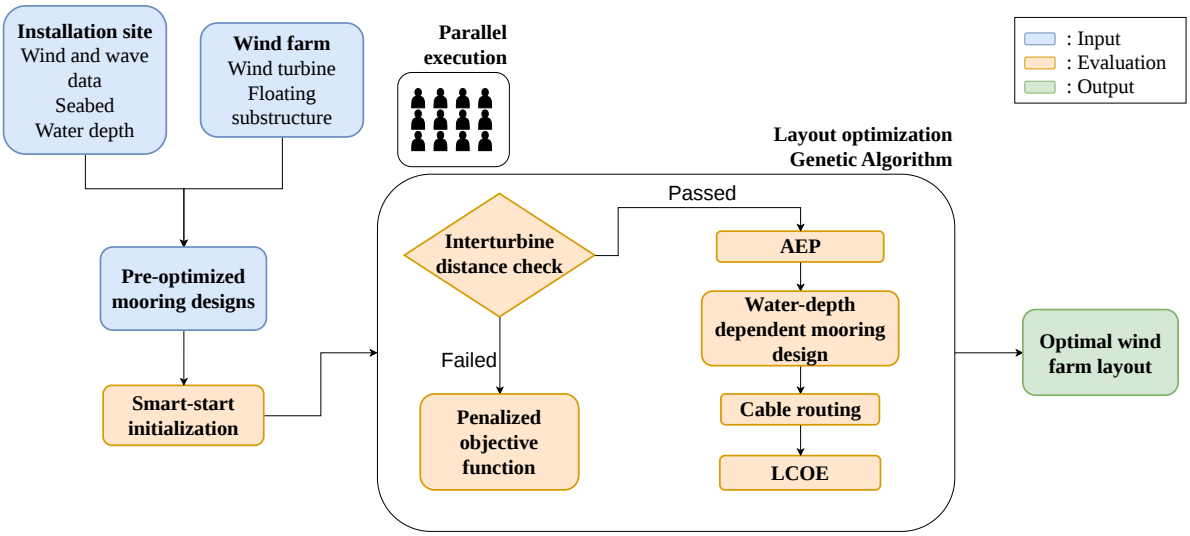



Figure 1: Flowchart of the integrated GA-based floating WFLO framework.

also used to pre-optimize mooring configurations over a range of water depths, generating a database of Pareto-optimal solutions queried during layout evaluation.

One high-AEP feasible layout is generated using the Smart-Start algorithm in PyWake [8], and it is used to initialize the GA population. Optimization uses MATLAB's single-objective GA with convergence- and generation-based termination conditions. Standard evolutionary operators (selection, crossover, mutation) are applied; power mutation and bounded exponential crossover are implemented according to [9, 10].

For each feasible layout, AEP is computed in PyWake using the Bastankhah–Porté-Agel wake model ($k = 0.05$) [11]. Mooring costs are interpolated from the precomputed Pareto fronts according to local water depth. The offshore substation is fixed at the centroid of turbine positions, after which inter-array cable routing is solved via the procedure described below. All cost components are combined in the economic model to compute the LCOE.

To benchmark performance, an RS algorithm implemented in TOPFARM is used as baseline [12, 13]. A schematic overview is provided in Figure 2. Starting from a Smart-Start generated layout, one turbine is randomly selected at each iteration and displaced by a random step in a random direction. Feasible candidates are evaluated using the same objective function pipeline as the GA framework, and a new layout is accepted only if it improves the incumbent LCOE. The procedure is repeated for a predefined number of iterations.

### *2.1 Inter-array cable routing optimization*

The IACRO problem is formulated as a nested optimization within both the GA and RS frameworks and modeled as a capacitated network design problem rooted at the substation. For a given layout, the node set is $\mathcal{N} = \{1, \ldots, N, s\}$ (including turbines and substation). Routing is solved on a complete directed graph with edge set $\mathcal{E} = \{(i, j) \in \mathcal{N} \times \mathcal{N} \,|\, i \neq j\}$ and edge weights $d_{ij}$, computed as the Euclidean distance between nodes $i, j$, ignoring bathymetry effects and dynamic cable sections at this stage.

A branched topology is assumed: each turbine is connected to exactly one downstream node, whereas the substation acts as the root node of the network and therefore has no downstream

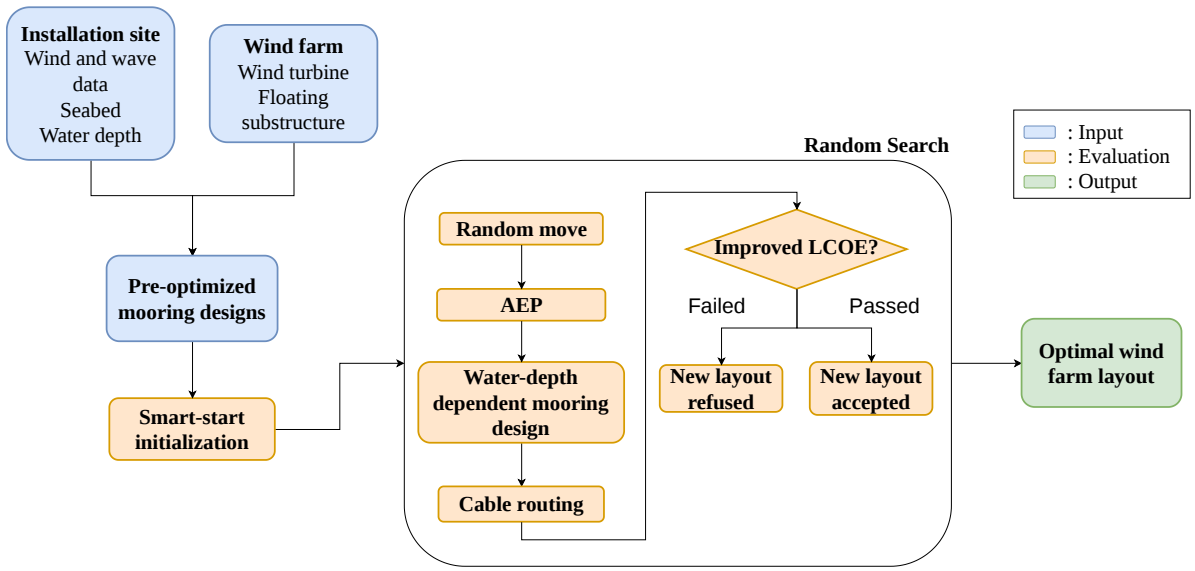



Figure 2: Flowchart of the baseline integrated RS-based floating WFLO framework.

connections. Electrical feasibility is enforced through branch capacity constraints:

$$f_{ij} \leq \mathrm{MVA}_{\mathrm{max}}^{(k)}, \tag{4}$$

where $f_{ij}$ is the aggregated rated power on branch $(i, j)$ and $\mathrm{MVA}_{\mathrm{max}}^{(k)}$ is the capacity of cable type $k$. The objective is to minimize the total inter-array cable length,

$$L_{\mathrm{IA}}(\mathbf{y}) = \sum_{(i,j)\in\mathcal{E}} d_{ij}\, y_{ij}, \qquad \min_{\mathbf{y}} L_{\mathrm{IA}}(\mathbf{y}), \tag{5}$$

with binary variables $y_{ij}$ indicating whether a connection is installed.

The problem is solved using the Esau-Williams heuristic in OptiWindNet [14], which generates high-quality solutions with very low computational effort. It constructs a minimum-cost tree by iteratively merging branches based on length savings while satisfying capacity constraints. Multiple cable types with different capacities and unit costs are available; the heuristic assigns the least-cost type meeting flow requirements, enabling cost differentiation within a primarily length-driven topology. After routing, cable cost is used in the economic model described below.

### *2.2 Water Depth-dependent Mooring Model*

A depth-dependent mooring model is integrated to capture the coupling between bathymetry and wind farm economics. Mooring configurations are pre-optimized over a discrete set of water depths and motion constraints, generating Pareto-optimal solution fronts that trade off capital expenditure (CAPEX) and platform performance. During layout optimization, these fronts are interpolated so that each turbine is assigned the minimum-CAPEX configuration satisfying local motion constraints. The construction of the Pareto-optimal mooring mapping is presented in [15], while its integration within a wind farm layout optimization framework is described in [16].

Pre-optimization addresses a multi-objective problem that minimizes mooring CAPEX and platform motions, following the approach in [17]. For a given floating substructure, which defines fairlead positions and number of lines, six design variables define the mooring configuration: anchor radius, stretching factor, line composition factor, rope material, rope diameter, and

chain nominal diameter. These variables allow catenary, semi-taut, and taut layouts, jointly determining system geometry, stiffness, and cost. Component modelling and cost estimation follow [18]. Mooring azimuthal orientation is not optimized at the farm scale.

For each design, quasi-static simulations evaluate platform motions and line tensions under two critical load cases (selected as in [19]): the maximum operative sea state, representing severe operational conditions with maximum thrust, and the ultimate limit state, representing extreme conditions with the rotor parked. Head-sea alignment of wind and waves is assumed. Feasibility requires satisfaction of safety and motion constraints; otherwise the design receives a penalized objective value.

A normed motions vector obtained from OrcaFlex simulations represents platform motions:

$$NMV_{SS} = \left\| \left( \frac{\phi_{SS}}{\phi_{max}}, \frac{x_{SS}}{x_{max}} \right) \right\|, \tag{6}$$

where $\phi$ and $x$ denote pitch and surge, respectively, and $SS$ identifies the sea state. The least-cost anchor is selected from a predefined set (*i.e.* drag embedded anchors, vertical load anchors, suction anchors, and driven piles) based on seabed compatibility and load angles following [18]. Pareto front designs thus represent optimal trade-offs between economic cost and motion performance. During layout evaluation, the Pareto database is queried and interpolated based on local water depth to assign each turbine the least-cost feasible mooring configuration.

### *2.3 Economic Cost Model*

The LCOE of the wind farm is evaluated as:

$$\text{LCOE} = \frac{\text{DEVEX} + \text{CAPEX} + \sum_{t=1}^{T} \frac{\text{OPEX}}{(1+r)^t} + \frac{\text{DECEX}}{(1+r)^T}}{\sum_{t=1}^{T} \frac{\text{AEP}}{(1+r)^t}}, \tag{7}$$

where DEVEX, CAPEX, OPEX, and DECEX denote development, capital, operational, and decommissioning expenditures, $r$ is the discount rate, and $T = 25$ years is the project lifetime. Mooring CAPEX depends on the positioning of the turbines via local water depth, while inter-array cable CAPEX is obtained from the nested IACRO.

Mooring costs are evaluated using a bottom-up model that links expenditures to physical system properties or duration of operations. Mooring system CAPEX is defined as the sum of costs for purchase and fabrication plus installation and commissioning. Purchase and fabrication costs are the sum of each i-th component cost $C_i$:

$$C_i = m \cdot c_i, \tag{8}$$

where $m$ is the component (line section or anchor) mass and $c_i$ the unit cost.

Installation and commissioning costs $C_{I\&C}$ combine pre-lay ($pl$) and hook-up ($hu$) operations:

$$C_{I\&C} = \sum_{v=1}^{V} \frac{t_{pl,v} N_A}{24} c_v N_v + \sum_{v=1}^{V} \frac{t_{hu,v}}{24} c_v N_v, \tag{9}$$

where $t_{pl}$ and $t_{hu}$ are operation times, $N_A$ the number of anchors, $c_v$ the vessel daily rate, and $N_v$ the number of vessels of type $v$. Anchor handling and tug support vessels are used for drag-embedded and vertical load anchors below 10 t, while larger anchors require an anchor handling vessel; suction anchors and driven piles use construction support vessels. All detailed component parametrization and cost derivation are consistent with [18].

The bottom-up approach is also applied to the inter-array cable network. Once routing is determined, total cable cost is:

$$C_{\mathrm{IA}} = \sum_{(i,j)\in\mathcal{E}^*} d_{ij} \cdot c_{ij}^{(k)}, \tag{10}$$

where $\mathcal{E}^*$ is the set of installed branches and $c_{ij}^{(k)}$ the unit cost of three-core AC cable type $k$ (including lay and burial). Dynamic cables and export cable costs are excluded due to limited data availability. Cable capacities and unit costs are reported in Table 1.

Table 1: Capacity and cost per unit mass of inter-array cable types (Adapted from: [20]).

| **Type** | Capacity [MVA] | Unit cost [€/m] | Cross-section [$mm^2$] |
|---|---|---|---|
| 1 | 49 | 514 | 300 |
| 2 | 75 | 793 | 800 |

The remaining CAPEX cost items as well as DEVEX, OPEX, and DECEX are modeled using a top-down formulation proportional to installed capacity, with unit costs derived from industry references [21].

## 3 Case Study: Deep-Water Site West of Sicily

The proposed frameworks are applied to a deep-water site west of Sicily (Italy), corresponding to the north-eastern Grecale lot of the MedWind project. The domain is approximated as a rectangular region bounded by 37.908°–38.029° N and 11.332°–11.440° E. Two bathymetric configurations are analyzed: a realistic bathymetry (RB) and a simplified gradient bathymetry (GB). In the RB case, depths are derived from the GEBCO 2025 grid [22] and range from approximately 460 m to 870 m, with deeper areas in the north-west and shallower areas toward the south-east. This spatial variability leads to substantial differences in turbine-level mooring costs. In the GB case, a monotonic west–east depth gradient is imposed over the same depth range, removing local irregularities while preserving the large-scale trend. This configuration isolates depth-driven effects on layout, cabling, and mooring interactions. The RB case is used to evaluate GA and RS performance under realistic seabed conditions, whereas the GB case provides a controlled benchmark for sensitivity analysis. Figures 3a and 3b show the bathymetry maps in local Cartesian coordinates. All other site characteristics are identical in both cases.

Hourly wind data at 100 m height from ERA5 database (2005–2024) [23] are used to derive the wind climate. Wind directions are discretized into twelve sectors and fitted with sector-wise Weibull distributions. The site is dominated by north-westerly winds with a secondary south-easterly component (Figure 4). For the wind turbine, the IEA 15 MW reference turbine [24], mounted on the VolturnUS-S semi-submersible platform [25], is adopted. Consistent with the platform design, three mooring lines spaced at 120° are assumed. Seabed properties from EMODNet [26] indicate predominantly mud to muddy sand conditions. For anchor selection and cost modeling, homogeneous medium-clay conditions are assumed following [18].

## 4 Results and discussion

This section presents results for the GB and RB case studies in terms of wind farm layout, LCOE, mooring, and cable costs. The GB case is first analyzed to highlight the effect of integrating depth-dependent mooring design and cable routing into the WFLO framework. The RB case is then used to compare the GA framework against the RS benchmark.

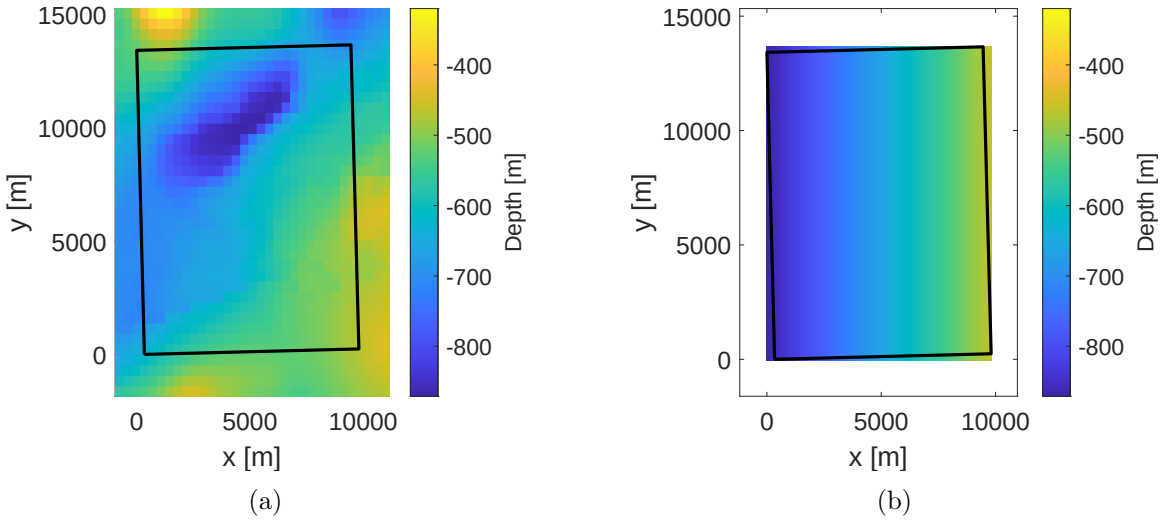



Figure 3: Bathymetry maps in local Cartesian coordinates: (a) RB case, GEBCO-derived bathymetry; (b) GB case, linear bathymetry gradient.

All simulations were initialized using the Smart-Start algorithm on a 31×41 grid. The GA was executed in parallel on 12 workers with a population of 200 individuals, a convergence tolerance of $10^{-5}$, and a maximum of 100 stall generations. These parameters slightly deviate from MATLAB default settings and were selected after preliminary tests to ensure stable convergence with moderate computational cost. The RS framework was executed for 3000 iterations, identified during preliminary tests as a suitable compromise between solution quality and runtime. Platform motion limits were set to 20 m surge and 10° pitch for both frameworks.

Figures 5 and 6 show the initialized and optimized layouts for the two case studies. Wind turbines are represented as triangles with dotted circles, whose radii correspond to five rotor diameters, while dashed circles indicate mooring anchor radii. For cases including IACRO, inter-array cables (red lines) and the offshore substation (square) are also shown. Numerical results are summarized in Table 2 as absolute values and percentage variations, grouped by case and optimization algorithm.

The GB case is first analyzed considering only turbine-specific mooring costs. As shown in Figures 5a and 5b, turbines migrate toward the shallower eastern region where mooring costs are lower. Because the available area is large, turbines remain widely spaced and AEP variations are negligible. However, mooring CAPEX decreases by 16.56%, resulting in a 0.81% reduction in LCOE. When IACRO is included, in Figures 5c and 5d, turbines are both attracted to shallower areas and packed more closely to shorten cable routes. The resulting topology maintains the general South-West to North-East branch alignment while reducing cable length. Despite a minor AEP reduction of 0.33%, LCOE decreases by 1.09%, driven by reductions of 19.21% in mooring CAPEX and 30.75% in cable CAPEX.

These results highlight the importance of integrating bathymetry-dependent mooring design and IACRO into WFLO. Although Smart-Start already provides near-optimal AEP, the integrated framework still yields noticeable LCOE reductions and layout changes. In the optimized GB configurations, moorings account for approximately 4.86% of total CAPEX (4.6% when cable costs are included), while cables contribute about 1.75%. The GB case therefore provides a qualitative upper bound on the benefits of integrated optimization.

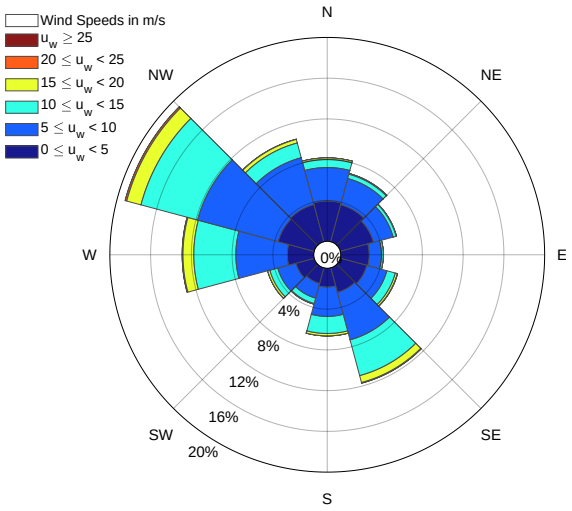



Figure 4: Case study wind rose derived from ERA5 hourly data (2005–2024).

Table 2: Layout optimization results for GB and RB cases using GA (with RS benchmark in RB). Percentage variations are relative to the initialized configuration.

| Case - | | | | AEP | | LCOE | | CF | | Moor. CAPEX | | Cab. CAPEX | |
|---|---|---|---|---|---|---|---|---|---|---|---|---|---|
| O.A. | Moor. | Cab. | Cfg. | [GWh] | [%] | [€/MWh] | [%] | [-] | [%] | [M€] | [%] | [M€] | [%] |
| GB - | | | | | | | | | | | | | |
| GA | ✓ | | INIT | 1047.2 | | 147.81 | | 39.85 | | 80.30 | | | |
| GA | ✓ | | OPT | 1047.9 | 0.06 | 146.62 | -0.81 | 39.87 | 0.05 | 67.00 | -16.56 | | |
| GA | ✓ | ✓ | INIT | 1048.4 | | 150.47 | | 39.89 | | 79.66 | | 35.35 | |
| GA | ✓ | ✓ | OPT | 1044.9 | -0.33 | 148.83 | -1.09 | 39.76 | -0.33 | 64.36 | -19.21 | 24.48 | -30.75 |
| RB - | | | | | | | | | | | | | |
| GA | ✓ | ✓ | INIT | 1049.5 | | 149.02 | | 39.94 | | 62.83 | | 36.3 | |
| RS | ✓ | ✓ | OPT | 1044.9 | -0.44 | 148.48 | -0.36 | 39.76 | -0.45 | 58.70 | -6.57 | 25.76 | -29.04 |
| GA | ✓ | ✓ | OPT | 1049.0 | -0.05 | 148.31 | -0.48 | 39.92 | -0.05 | 60.35 | -3.95 | 29.16 | -19.67 |

The RB case compares GA and RS performance under realistic bathymetry. As shown in Table 2, both algorithms reduce LCOE relative to the initialized layout while maintaining nearly unchanged AEP. The GA achieves the lowest LCOE, whereas RS yields larger reductions in individual CAPEX components. In the GA solution, mooring and cable costs decrease by about 4% and 20%, respectively. Although smaller than in the GB case, these reductions remain economically significant. Moorings account for 4.31% and cables for 2.08% of total CAPEX in the GA solution, compared with 4.21% and 1.84% for RS, consistent with the GB case.

The optimized layouts show consistent spatial patterns. Turbines tend to move toward shallower areas along the site boundaries, while internal turbines maintain alignments that reduce wake interactions. This behavior reflects the combined influence of wake effects, bathymetry, and cable routing observed in the GB analysis.

From a computational perspective, the GA also demonstrates advantages in exploration capability and parallel performance. In the present simulations, it evaluated approximately 40 000 candidate layouts compared to 3 000 evaluations for RS, while requiring about 9 minutes per run versus 18 minutes for RS.

Both algorithms may converge to local optima. Multiple runs during testing produced layouts with similar LCOE values but different spatial configurations, indicating that several layouts can

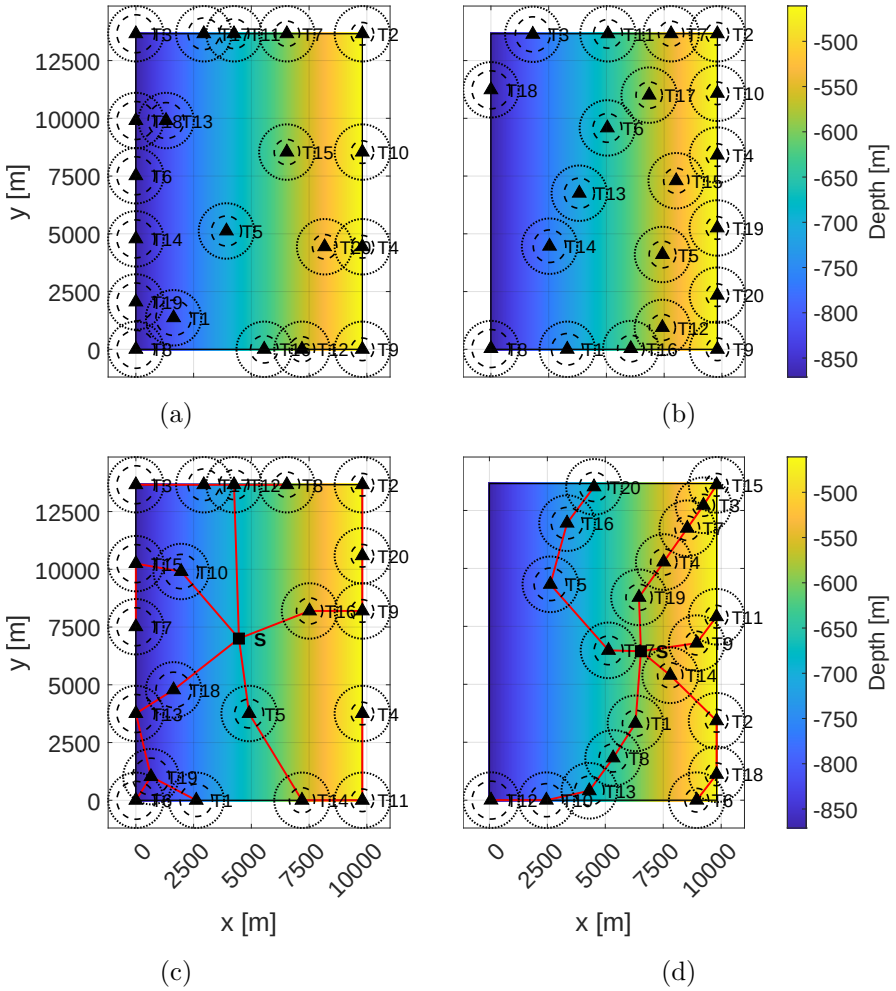



Figure 5: GB case wind farm layouts: (a) initialized with moorings; (b) GA-optimized with moorings; (c) initialized with moorings and cables; (d) GA-optimized with moorings and cables.

yield comparable techno-economic performance. The RS framework tends to produce tighter packing along site boundaries or orthogonal to the prevailing wind direction, which can slightly reduce AEP and limit its final performance relative to GA.

Some limitations of the proposed framework should be noted. First, the case study involves a relatively small number of turbines relative to the available area, resulting in large inter-turbine spacing and limited wake losses. Consequently, the Smart-Start algorithm already yields near-optimal AEP layouts. Future work should consider denser layouts or larger turbine counts to better assess optimization performance. Second, the electrical system model assumes the offshore substation is located at the centroid of turbine positions. This can lead to unrealistic proximity between the substation and turbines, artificially reducing cable lengths and associated costs. Future extensions should enforce minimum separation constraints and explicitly optimize substation placement. Finally, scaling the GA to larger wind farms may be challenging due to the linear growth in decision variables with turbine count. Future work should investigate scalability and global optimality guarantees, *e.g.* through alternative optimization strategies, local refinements, or multi-objective formulations to better discriminate between solutions with similar LCOE.

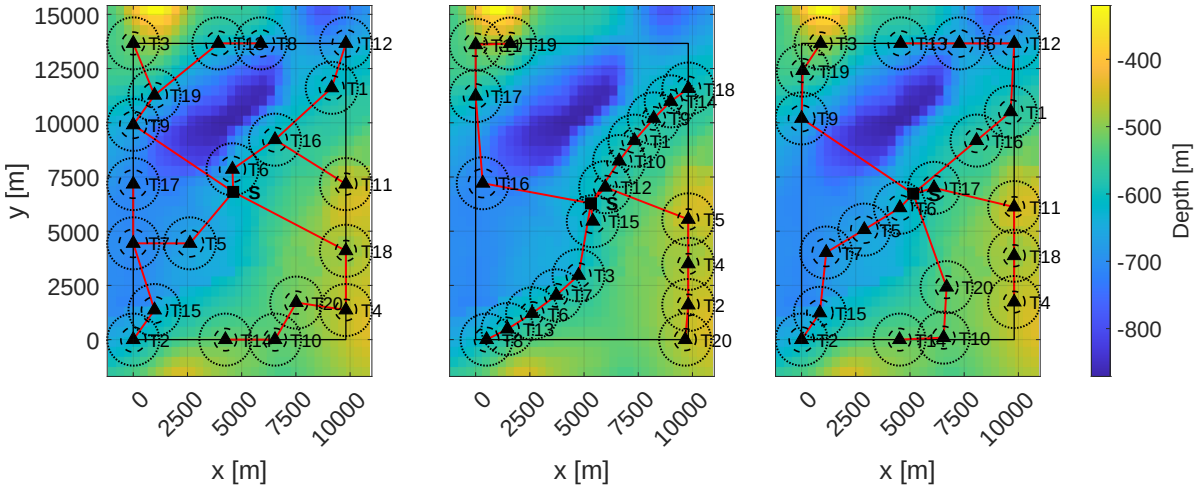



Figure 6: RB case wind farm layouts: (a) initialized; (b) RS-optimized; (c) GA-optimized.

## 5 Conclusions

This work addressed the floating WFLO problem by integrating AEP, IACRO, and water-depth-dependent, turbine-specific mooring system optimization within a unified framework. A GA was developed to solve the resulting bounded continuous optimization problem. Application to an artificial gradient bathymetry case highlighted the strong coupling between layout, cabling, and mooring design, and its impact on the final configuration and LCOE. The realistic deep-water Mediterranean case further demonstrated the framework's applicability under complex bathymetric conditions, where spatial depth variability can be exploited in the optimization process. Benchmarking against a RS baseline showed that the GA achieves better performance with higher computational efficiency. In the realistic case, the optimized solution yields a 0.48% reduction in LCOE, driven by decreases of 3.95% in mooring system cost and 19.67% in inter-array cable cost.

Future work should focus on improving scalability for larger wind farms and enhancing global search capabilities, performing cost sensitivity analyses to clarify the relative influence of moor-ing and electrical systems, and extending the framework toward multi-objective formulations, including integrated offshore substation placement and anchor-sharing strategies.

## Acknowledgments

Lorenzo Dutto expresses his gratitude for the funds received from the Ministry of University and Research and PNRR's PhD scholarship program defined in DM-118/2023. This publication is part of the project PNRR-NGEU. Paula B. Garcia-Rosa was supported by the Norwegian Research Centre on Wind Energy, FME Northwind, WP3 "Electrical Infrastructure & System Integration", funded by the Research Council of Norway under Project 321954.

## References

[1] International Energy Agency (IEA), "World energy outlook 2025," 11 2025.

[2] H. Sun *et al.*, "Investigation of floating offshore wind farm layout optimization considering mooring line constraints," *J. Mar. Sci. Eng.*, vol. 13, no. 1, 2025.

[3] M. Hall *et al.*, "Floating wind farm layout optimization considering moorings and seabed variations," *J. Phys. Conf. Ser.*, vol. 2767, p. 062038, jun 2024.

[4] L. Sirkis *et al.*, "Floating offshore wind farm array optimization considering mooring lines, anchors, and array cables," in *Offshore Technol. Conf.*, OTC, 4 2025.

[5] S. Tao *et al.*, "Nonuniform wind farm layout optimization: A state-of-the-art review," *Energy*, vol. 209, p. 118339, 2020.

[6] J. J. Thomas *et al.*, "A comparison of eight optimization methods applied to a wind farm layout optimization problem," *Wind Energy Sci.*, vol. 8, no. 5, pp. 865–891, 2023.

[7] M. Kallinger *et al.*, "Offshore electrical grid layout optimization for floating wind—a review," *Clean Technol.*, vol. 5, no. 3, pp. 791–827, 2023.

[8] R. Valotta Rodrigues *et al.*, "Speeding up large-wind-farm layout optimization using gradients, parallelization, and a heuristic algorithm for the initial layout," *Wind Energy Sci.*, vol. 9, no. 2, pp. 321–341, 2024.

[9] T. Yokota *et al.*, "Genetic algorithm for non-linear mixed integer programming problems and its applications," *Comput. Ind. Eng.*, vol. 30, no. 4, pp. 905–917, 1996.

[10] H. Jalota and M. Thakur, "Genetic algorithm designed for solving linear or nonlinear mixed-integer constrained optimization problems," in *Int. Proc. Adv. Soft Comput., Intell. Syst. Appl.*, pp. 277–290, Springer Singapore, 2018.

[11] M. Bastankhah and F. Porté-Agel, "A new analytical model for wind-turbine wakes," *Renewable Energy*, vol. 70, pp. 116–123, 2014.

[12] M. Pedersen *et al.*, "Dtuwindenergy/topfarm2: Release of v2.6.1," Nov. 2025.

[13] J. Feng and W. Shen, "Solving the wind farm layout optimization problem using random search algorithm," *Renewable Energy*, vol. 78, pp. 182–192, 2015.

[14] M. Souza de Alencar *et al.*, "Dtuwindenergy/optiwindnet: Optiwindnet v0.1.6," Jan. 2026.

[15] F. Niosi *et al.*, "Site-specific mooring design guidelines for utility-scale floating wind," in *Proceedings of the ASME 2026 45th Int. Conf. Ocean, Offshore Arctic Eng.*, 2026.

[16] L. Dutto *et al.*, "On the effect of turbine-specific mooring system design on floating offshore wind farm layout optimization," in *Proceedings of the ASME 2026 45th Int. Conf. Ocean, Offshore Arctic Eng.*, 2026.

[17] F. Niosi *et al.*, "Experimental investigation of taut leg moored fowts in damaged conditions," in *Innovations in Renewable Energies Offshore*, pp. 419–425, 2024.

[18] L. Dutto *et al.*, "A decision making strategy for cost-effective anchoring and mooring design in floating offshore wind systems," *Ocean Engineering*, vol. 353, p. 124768, 2026.

[19] F. Niosi *et al.*, "Experimental investigation and dataset release of a taut-leg mooring system for a semi-submersible floating offshore wind turbine," *Ocean Eng.*, vol. 328, p. 121067, 2025.

[20] T. Treider *et al.*, "Cost-saving potential of utilizing a shared electrical connection to shore for an offshore wind farm and a cluster of oil and gas platforms," *J. Phys. Conf. Ser.*, vol. 3131, p. 012019, oct 2025.

[21] BVGAssociates, "Guide to a floating offshore wind farm," 2025.

[22] GEBCO Compilation Group, "Gebco 2025 grid," 2025.

[23] H. Hersbach *et al.*, "Era5 hourly data on single levels from 1940 to present." Copernicus Climate Change Service (C3S) Climate Data Store (CDS), 2023. Accessed on 17-12-2025.

[24] E. Gaertner *et al.*, "Iea wind tcp task 37: Definition of the iea 15-megawatt offshore reference wind turbine," tech. rep., National Renewable Energy Laboratory (NREL), 3 2020.

[25] C. Allen *et al.*, "Definition of the umaine volturnus-s reference platform developed for the iea wind 15-megawatt offshore reference wind turbine," tech. rep., NREL, 7 2020.

[26] A. Kaskela *et al.*, "Picking up the pieces—harmonising and collating seabed substrate data for european maritime areas," *Geosciences*, vol. 9, p. 84, 2 2019.